

## Impact ionization in InSb probed by THz-pump THz-probe spectroscopy

Matthias C. Homann,<sup>1</sup> Janos Hebling,<sup>2</sup> Harold Y. Hwang,<sup>1</sup> Ka-Lo Yeh,<sup>1</sup> and Keith A. Nelson<sup>1</sup><sup>1</sup>Massachusetts Institute of Technology<sup>2</sup>Department of Physics, University of Pecs, Hungary

(Dated: February 21, 2024)

Picosecond carrier dynamics in indium antimonide (InSb) following excitation by below-bandgap broadband far infrared radiation were investigated at 200 K and 80 K. Using a novel THz-pump/THz-probe scheme with pump THz fields of 100 kV/cm and an intensity of 100 MW/cm<sup>2</sup>, we observed carrier heating and impact ionization. The number of carriers produced exceeds 10<sup>16</sup> cm<sup>-3</sup>, corresponding to a change in carrier density  $N = N_0$  of 700% at 80 K. The onset of a well defined absorption peak at 1.2 THz is an indication of changes in LO and LA phonon populations due to cooling of the hot electrons.

PACS numbers: 78.47.J-, 71.55.Eq, 72.20.Ht, 72.20.Jv, 42.65.Re

Hot electron dynamics and carrier multiplication in semiconductors play important roles in the design of fast electronic devices as well as in the development of highly efficient solar cells [1]. The elucidation of carrier dynamics on the ultrashort timescale is hence of great technological as well as fundamental interest. Indium antimonide (InSb) is a model system for the study of hot electron dynamics due to its low bandgap of 170 meV at room temperature [2] and the fact that it has the highest electron mobility and saturation velocity of all known semiconductors. Its high mobility allows the fabrication of transistors with extremely high switching speed, [3] but further technological applications are complicated by the low impact ionization threshold. Impact ionization by high electric fields is a well known phenomenon in InSb [4] and has been studied mostly in the quasi-DC limit of  $\tau \gg \tau_{relax}$  where  $\tau$  is the characteristic electron momentum relaxation time, typically of the order of a few picoseconds. In this limit, the extent of impact ionization is determined by the probability of an electron gaining enough energy from the driving field to cross the ionization threshold. An equilibrium between energy gain of the electrons due to the accelerating field and energy loss due to phonon scattering is reached, leading to saturation in the drift velocity  $v_d$ . Carriers with energies greater than the bandgap  $E_g$  can produce new electron-hole pairs through the impact ionization process, which also can be viewed as an inverse Auger effect [5]. The newly generated carriers can be accelerated by the field and can induce impact ionization themselves. Carrier relaxation dynamics in the high-frequency limit ( $\tau \ll \tau_{relax}$ ) have been studied in InSb by sub-picosecond time-resolved mid-infrared nonlinear spectroscopy using above-bandgap excitation [6]. Below-bandgap excitation by CO<sub>2</sub> lasers also has been used for time-resolved measurements with nanosecond resolution [7] and for intensity-dependent transmission measurements [8, 9]. Below-bandgap excitation allows study of bulk hot-carrier dynamics without optical generation of holes or strong absorption and high carrier densities

very close to the surface.

In this letter, we report experimental observations of carrier generation in InSb at 80 K and 200 K due to impact ionization induced by below-bandgap IR radiation on the picosecond time scale, where  $\tau \ll \tau_{relax}$ . Near single-cycle pulses with field strengths up to 100 kV/cm and a duration of 1 ps were used. The rise time of the THz pulses was less than the electron momentum relaxation time of  $\tau = 2.5$  ps in InSb at 77 K. This leads to highly accelerated carriers that can cause carrier multiplication through impact ionization [10, 11]. THz radiation also can be used as a very sensitive probe to directly monitor free carrier behavior in semiconductors [12]. The combination of sub-bandgap direct excitation of doped semiconductors and time-resolved spectroscopy provides an excellent tool for observing carrier dynamics [10, 13, 14].

The experimental setup shown in Figure 1 was used for collinear THz-pump/THz-probe measurements. We generated single-cycle THz pulses by optical rectification of a 800 nm, 5.5 mJ pulse from a Ti:Sapphire laser with 100 fs pulse duration at a repetition rate of 1 kHz. We tilted the pulse intensity front with a grating-lens combination to achieve noncollinear velocity matching in lithium niobate [15, 16], yielding THz pulses with energies up to 3 J [17, 18]. The optical beam was split using a 10:90 beam splitter into two parts that were recombined under a small angle at the same spot on the grating. The 10% part was modulated using an optical chopper and was used to generate the THz probe. The 90% part was variably delayed and was used to generate the THz pump pulse. The single-cycle THz pulses were focused onto the sample using a 90-degree  $\phi$ -axis parabolic mirror pair with 190 and 75 mm focal lengths. The focused size was determined to be 1 mm using a razor blade scan. Another  $\phi$ -axis parabolic mirror pair with focal lengths of 100 and 190 mm was used to image the sample plane onto the ZnTe detector crystal for electro-optic sampling of the THz field using balanced detection and a lock-in amplifier [19]. In order to ensure the linearity of the detected signal and to eliminate THz pulse re-

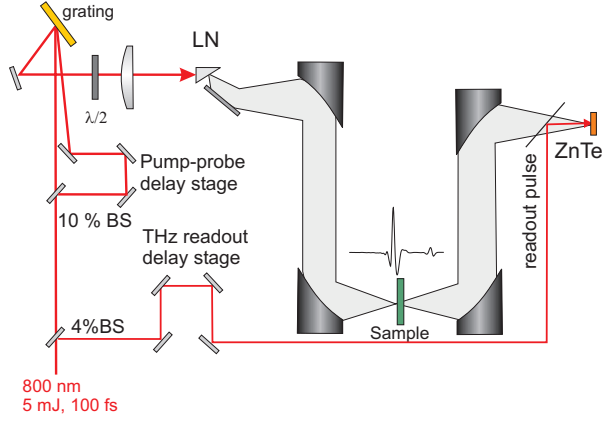


FIG. 1: The experimental setup uses pump and probe THz pulses in a collinear geometry, generated by tilted pulse front excitation in  $\text{LiNbO}_3$  (LN)

tions [20], the ZnTe sampling crystal had an active layer of 0.1 mm and a total thickness of 1.1 mm. Selective chopping of the probe beam provided excellent suppression of the pump pulse. Spectral analysis of our THz pump-probe results was conducted in the 0.2 to 1.6 THz range where the spectral amplitude was sufficiently high. A pair of wiregrid polarizers was used to attenuate the THz pulses for intensity-dependent studies. The samples were a n-type Te-doped and a nominally undoped InSb wafer, each 450  $\mu\text{m}$  thick, with carrier concentrations at 77 K of  $2.0 \times 10^{15} \text{cm}^{-3}$  and  $2.0 \times 10^{14} \text{cm}^{-3}$  respectively. The mobility as specified by the manufacturer was  $2.5 \times 10^5 \text{cm}^2/\text{Vs}$ . The THz fields were polarized parallel to the (100) axes of the crystals. We measured the THz fields  $E(t)$  that reached the ZnTe crystal with and without the sample in the beam path from which we calculated the effective absorption coefficient

$$\alpha_e = \frac{1}{d} \ln T^2 \frac{\int_0^{t_{\text{max}}} E_{\text{sam}}^2(t) dt}{\int_0^{t_{\text{max}}} E_{\text{ref}}^2(t) dt} \quad (1)$$

where  $d$  is the sample thickness,  $t_{\text{max}}$  is the time window of the measurement and  $T$  is a factor accounting for reflection losses at the sample surfaces. The quantity  $\alpha_e$  is equivalent to the energy absorption coefficient averaged over our bandwidth. Figure 2 shows the time-resolved absorption traces for the doped sample at 80 K and 200 K covering a probe delay range of up to 30 ps. At both temperatures, the absorption increases after THz excitation and reaches a plateau after 30 ps, with a total increase in absorption of 80–90  $\text{cm}^{-1}$ . This rise is caused by the generation of new carriers through impact ionization. Unique to the measurement at 200 K is the initial dip in the absorption immediately after the THz excitation. The drop in absorption in this case is caused by a decrease in the mobility of the highly energetic hot electrons as a result of both the strong non-parabolicity of the valley in the conduction band of

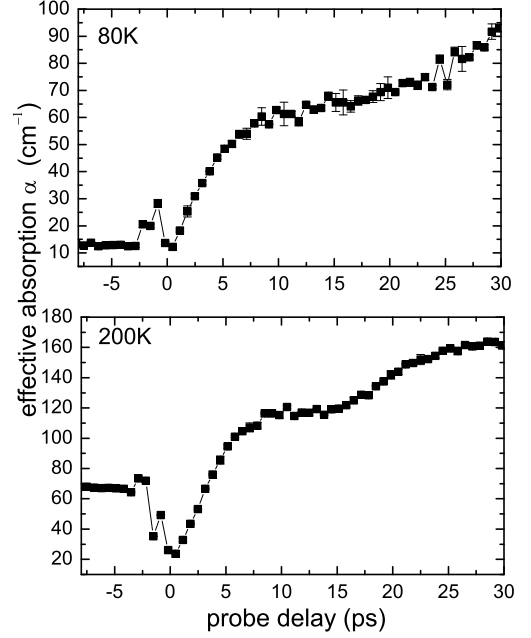


FIG. 2: THz-pump/THz-probe time-resolved absorption data, spectrally averaged over the 0.2–1.6 THz range, from doped InSb ( $N_c = 2.0 \times 10^{15} \text{cm}^{-3}$ ) at 80 K and 200 K. The deviation starting at 10 ps is due to re-heating caused by the THz pulse reflection within the sample.

InSb [21] and scattering of these hot electrons into side valleys [13, 14, 22, 23]. The carrier mobility directly influences the absorption coefficient which is typically conceptualized by the Drude model, parameterized by the plasma frequency  $\omega_p = (Ne^2/\epsilon_0 m)^{1/2}$  and the momentum scattering rate in the form

$$= \frac{1}{nc(\omega_p^2 + \gamma^2)}; \quad (2)$$

where  $\omega_1$  is the high-frequency limit of the dielectric function and  $n$  is the refractive index. In the low-frequency limit ( $\omega \rightarrow 0$ ) the absorption is directly proportional to the carrier mobility  $\mu = e/m$ . Due to the small bandgap of InSb, the intrinsic carrier concentration at 200 K is much higher than that at 80 K. The effect of absorption saturation is thus much stronger at 200 K. After 4 ps, the additional absorption caused by the newly generated carriers exceeds the saturation effect, the magnitude of which is also diminishing as a result of the cooling of the hot carriers, thereby leading to the delayed rise observed in the overall absorption.

Comparison between the equilibrium absorption of InSb at 80 K and the value measured 30 ps after intense THz excitation shows a eight-fold increase, indicating a similar increase in carrier concentration from  $2 \times 10^{15} \text{cm}^{-3}$  to  $1.5 \times 10^{16} \text{cm}^{-3}$ . The same analysis cannot be

applied reliably at 200 K due to the very large intrinsic carrier absorption, which overwhelms the dynamic range of our spectrometer system. This effect is especially acute at low frequencies where the absorption is strongest, leading to an apparent saturation of the frequency-averaged absorption shown in Figure 2b. Some signal at  $t < 0$  appears in Fig. 2a because of the nonlinear interaction in the LN crystal between the THz pump and probe fields and the optical pulses that generate them as well as nonlinear interactions in the sample.

We employ a simple system of rate equations, displayed below, to model the dynamics of impact ionization in the first 30 ps, assuming quadratic scaling [5] of the impact ionization probability above the threshold energy  $\epsilon_{th}$ .

$$\frac{dN}{dt} = C (\epsilon(t) - \epsilon_{th})^2 N(t) - (\epsilon(t) - \epsilon_{th}) \quad (3)$$

$$\frac{d\epsilon}{dt} = C (\epsilon(t) - \epsilon_{th})^2 \epsilon_{th} - (\epsilon(t) - \epsilon_{th}) \frac{\epsilon}{\epsilon_{th}} \quad (4)$$

In this model  $N(t)$  is the electron concentration,  $\epsilon(t)$  is the average carrier energy and  $\epsilon(t)$  is the Heaviside step function. We used a numerical value of  $C = 7 \times 10^{20} \text{ J}^{-2} \text{ s}^{-1}$  obtained from Ref. [24]. The energy relaxation time  $\tau_e$  was assumed to be time and energy independent.

A numerical solution, taking into account the reflection at the sample interface, is shown in Fig. 3. The effect of absorption saturation due to carrier heating [13, 14] was accounted for approximately by assuming  $\epsilon_{eff} / N(t) \epsilon_0 = \epsilon(t) / \epsilon_0$  where  $\epsilon_0$  is the average carrier energy immediately after excitation. From this fit we obtain a phenomenological relaxation time  $\tau_{eff}$  of 7 ps, much longer than the 1.3-2 ps calculated for the energy relaxation time in the DC limit by Kobayashi [25]. The faster value cannot describe our experimental conditions since it would preclude impact ionization and carrier cooling dynamics that we observe at slower time scales. In order to elucidate the lattice dynamics further, we performed a series of intensity-dependent pump-probe measurements with a fixed probe delay. Figure 4 shows the absorption spectra obtained with different pump intensities at a probe delay of 35 ps for the doped and undoped samples at 80 K. At frequencies below 0.6 THz, we observe the expected Drude-like contribution from free carrier absorption which is more pronounced at higher pump fluence. In addition, we observe a distinct absorption peak at 1.2 THz in the undoped sample and a weak feature that indicates a similar peak in the doped sample. The amplitude of the peak is highly intensity dependent, and appears to approach its asymptotic value just above 50% of the maximum intensity. The behavior of this peak suggests that its origin is lattice vibrational rather than electronic. Polar optical phonon scattering is well known as the dominant energy loss mechanism for hot electrons in InSb [26]. The main channel of energy

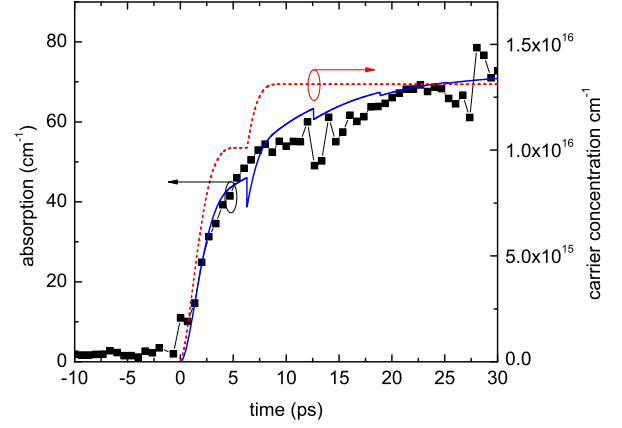


FIG. 3: Experimental data for the undoped sample (squares) and simulation results for the carrier concentration (dashed) and absorption (solid line) based on quadratic scaling of impact ionization rate with carrier energy. Parameters used were:  $N(t=0) = 5 \times 10^{13} \text{ cm}^{-3}$ , energy relaxation time  $\tau_e = 7 \text{ ps}$  and  $\epsilon_0 = \epsilon(t=0) = 1.3 \text{ eV}$ .

loss is through the emission of LO phonons with a frequency of 5.94 THz. These phonons decay into acoustic modes through anharmonic terms of the crystal potential and through the second-order electric moment of the lattice [27]. A series of sum- and difference phonon peaks between 1 to 10 THz has been observed and assigned in the far-infrared spectrum of InSb [28]. At very low THz fields, produced by a photoconductive antenna, we also were able to observe some of these weak absorption peaks in the undoped sample. The assignments reported in [28] indicate a 1.2 THz difference frequency between the LO and LA mode at the zone boundary. The drastic change in the absorption coefficient of the difference phonon peak is the result of large changes in phonon populations due to energy transfer from the hot electrons generated by the THz pump pulse. Monte-Carlo simulations [29] have shown that substantial phonon population changes can occur even at comparatively low DC fields on picosecond timescales. The temporal evolution of the electron-lattice interaction can be studied by separating the spectrally resolved pump-probe data into two different frequency bands 0.2-0.6 THz and 1.0-1.2 THz. This is illustrated in Figure 5 where data from time-resolved measurements at full THz intensity and at half the full intensity are shown for the doped sample. For the low-frequency band, the rise in absorption is almost identical at the two intensities, while the contribution from the absorption between 1.0 to 1.2 THz is reduced considerably when the THz intensity is halved. The higher frequency portion of the absorption spectrum is clearly more sensitive to the intensity of the THz pump pulse, as illustrated

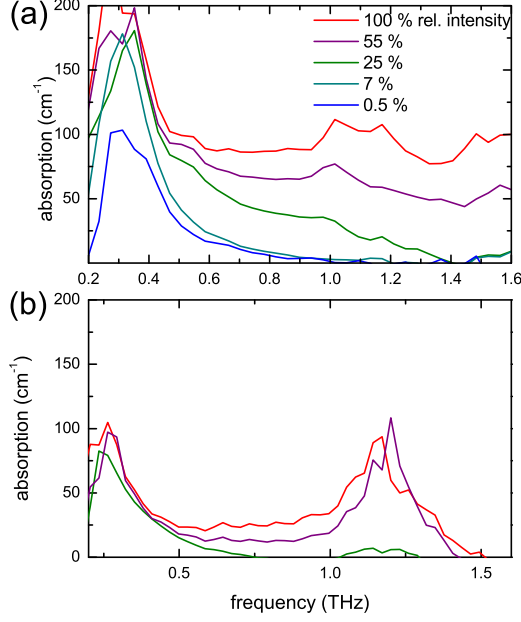


FIG. 4: THz absorption spectra at various pump intensities measured at a probe delay time of 35 ps for the doped sample (a) and undoped sample (b) at 80 K

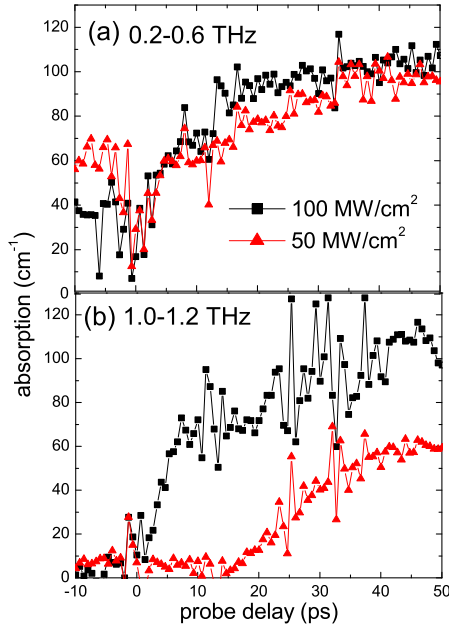


FIG. 5: Time-resolved spectrally averaged absorption for the doped sample at 80 K with 100% pump intensity (black squares) and 50% pump intensity (red triangles). (a) the average absorption between 0.2 and 0.6 THz, (b) the average absorption between 1.0-1.2 THz

in Figure 4b. In addition, at the lower intensity there is a delay of approximately 10 ps before the rise of the absorption signal. This delay was reproduced qualitatively for all measurements at intermediate THz pump levels. We do not have a complete understanding of the intensity-dependence of the delay, but we note that the delay is on the order of the LO phonon decay time in InSb [27], suggesting that it arises from electronic and LO phonon relaxation processes that populate the LA phonons. The large fluctuations observed at 12 and 24 ps are due to THz pump pulse reflections in the sample that are overlapped in the EO crystal with the THz probe pulse.

The newly developed THz pump/THz probe technique permits sensitive monitoring of carrier dynamics in semiconductors on the picosecond timescale. We observed the dynamics of impact ionization and carrier generation, up to a seven-fold increase over the equilibrium carrier-generation, following intense THz excitation of InSb. Our ability to spectrally analyze the time-resolved signal allowed us to detect distinct features that we attribute to decay of electronic energy into LO and LA modes. Monte-Carlo simulations are needed for a more in-depth understanding of the interplay between hot electrons and lattice, taking into account effects like impact ionization, intervalley- and polar optical phonon scattering and changes in phonon population. Additional effects of the THz fields themselves, including the possibility of THz-induced band-to-band tunneling [30] that could produce new carriers directly, also warrants further analysis.

We would like to thank R. Brazis for stimulating discussions. This work was supported in part by ONR grant no. N00014-06-1-0463.

mch@m.it.edu

- [1] J. H. Wemer, R. Brendel, and H.-J. Queisser, Appl. Phys. Lett. 67, 1028 (1995).
- [2] C. L. Little and D. G. Sella, Appl. Phys. Lett. 46, 986 (1985).
- [3] T. Ashley, in Proc. 7th Intl. Solid State and Integrated Circuits Tech. Conf., Beijing, China (2004).
- [4] C. L. Dick and B. Ancker-Johnson, Phys. Rev. B 5, 526 (1972).
- [5] L. V. Keldysh, Sov. Physics, JETP 21, 1135 (1965).
- [6] A. Lobad and L. A. Schlie, J. Appl. Phys. 95, 97 (2004).
- [7] T. W. Nee, C. D. Cantrell, J. F. Scott, and M. O. Scully, Phys. Rev. B 17, 3936 (1978).
- [8] S. D. Ganichev, A. P. Dmitriyev, S. A. Emelyanov, Ya, V. Terent'ev, I. D. Yaroshetskii, and I. N. Yassievich, Sov. Phys. JETP 63, 256 (1986).
- [9] S. D. Ganichev, J. Diener, and W. Prettl, Appl. Phys. Lett. 64, 1977 (1994).
- [10] M. C. Homann, J. Hebling, H. Y. Hwang, K. L. Yeh, and K. Nelson, in Ultrafast Phenomena XVI, edited by P. Corkum, S. de Silvestri, K. A. Nelson, E. Riedle, and R. W. Schoenlein (Springer, 2008).
- [11] H. Wen, M. Wiczner, and A. M. Lindenberg, Phys. Rev.

- B 78, 125203 (2008).
- [12] M . C . Beard, G . M . Turner, and C . A . Schmuttenmaer, Phys. Rev. B 62, 15764 (2000).
- [13] J. Hebling, M . C . Hermann, H . Y . Hwang, K .-L . Yeh, and K . A . Nelson, in Ultrafast Phenomena XVI, edited by P. Corkum, S. de Silvestri, K . A . Nelson, E. Riedle, and R. W. Schoenlein (Springer, 2008).
- [14] J. Hebling, M . C . Hermann, H . Y . Hwang, K .-L . Yeh, and K . A . Nelson (2008), in preparation.
- [15] J. Hebling, G . A. Masi, I. Kozma, and J. Kuhl, Optics Express 10, 1161 (2002).
- [16] T. Feurer, N. S. Stoyanov, D . W . Ward, J. Vaughan, E. R. Statz, and K . A . Nelson, Annu. Rev. Mater. Res. 37, 317 (2007).
- [17] K .-L . Yeh, J. Hebling, M . C . Hermann, and K . A . Nelson, Opt. Commun. 281, 3567 (2008).
- [18] K .-L . Yeh, M . C . Hermann, J. Hebling, and K . A . Nelson, Appl. Phys. Lett. 90, 171121 (2007).
- [19] Q . Wu and X .-C . Zhang, Appl. Phys. Lett. 67, 3523 (1995).
- [20] D . Turchinovich and J. I. Dijkhuis, Opt. Commun. 270, 96 (2007).
- [21] X . M . Weng and X . Lei, Phys. Stat. Solid. B 187, 579 (1995).
- [22] A . Mayer and F. Keilmann, Phys. Rev. B 33, 6962 (1986).
- [23] E. Constant, in Hot Electron Transport in Semiconductors, edited by L. Reggiani (Springer, 1985).
- [24] J. T. Devreese, R. G. van Welzenis, and R. P. Evrard, Appl. Phys. A 29, 125 (1982).
- [25] T. Kobayashi, J. Appl. Phys. 48, 3154 (1977).
- [26] E. M. Conwell, Solid State Physics, Suppl. 9 (Academic Press, New York, 1967).
- [27] D . Ferry, Phys. Rev. B 9, 4277 (1974).
- [28] E. S. Koteles, W . R. Datar, and G . Dolling, Phys. Rev. B 9, 572 (1974).
- [29] R. Brazis and R. Ragotis, Opt. Quant. Electron. 40, 249252 (2008).
- [30] E. O. Kane, J. Phys. Chem. Solids 12, 181 (1959).